Int J Adv Manuf Technol (2014) 74:995–1004
DOI 10.1007/s00170-014-6047-5

ORIGINAL ARTICLE

Investigating the effects of cross wedge rolling tool parameters on formability of Nimonic® 80A and Nimonic® 115 superalloys

S. Javid Mirahmadi · Mohsen Hamedi · Shahabeddin Ajami

Received: 21 September 2013 / Accepted: 5 June 2014 / Published online: 17 June 2014

Abstract Ni-base superalloys are a class of materials with high temperature excellent tensile, creep, and corrosion properties that have widespread applications in manufacturing hot parts of gas turbines. Application of cross wedge rolling (CWR) process for manufacturing Ni-base superalloys is of least investigated areas. In this article, the effects of CWR tool parameters on formability of Nimonic® 80A and Nimonic® 115 wrought superalloys are presented. The normalized Cockcroft-Latham model is adopted through finite element analysis to predict the occurrence of internal burst. The analytical results are validated through comparing them with experimental data. Comprehensive results of the effects of various CWR tool parameters on formability of Nimonic® 80A and Nimonic® 115 are presented. The results show that in some cases for Nimonic® 115, regardless of the stretching angle value (β), the internal burst fails the process. The results also indicate that Nimonic® 80A displays a relatively good ductility in low wedge angles and low stretching angles without suffering internal bursts, leading to sound part.

Keywords Cross wedge rolling · Ni-base superalloys · Critical damage · Normalized Cockcroft-Latham damage model

S. J. Mirahmadi (✉) · M. Hamedi
School of Mechanical Engineering, College of Engineering, University of Tehran, Tehran, Iran
e-mail: j.mirahmadi@ut.ac.ir

S. J. Mirahmadi · S. Ajami
R&D Department, Mavadkaran Engineering Company (MAPNA Group), Tehran, Iran

M. Hamedi
MAPNA R&D, Tehran, Iran

1 Introduction

Cross wedge rolling (CWR) is a metal forming process that is used to form axisymmetric parts or forging preforms [1]. This process is known for its high productivity and low waste of raw material. Despite these benefits, because of complex nature of deformation and failure mechanisms in this process, this process is not widespread for manufacturing parts [2]. In recent years, many authors have studied different aspects of CWR process. Pater gave a method to determine the mean unit contact pressure according to basic process parameters [3]. Lovell presented an analytical method to evaluate the friction condition that prevents the slip of workpiece between tools [4]. Pater numerically studied the CWR including upsetting to determine the rolling force, contact surface, and rolling radius [5]. Deng et al. also studied the effect of material properties and velocity on slipping of the workpiece [6]. Slipping, necking, and internal bursts are common defects in CWR process that were investigated by Li et al. [7]. Pater presented an optimization method for the designing of the CWR tool [8]. Li and Lovell by using finite element method (FEM) model and experiments investigated the mechanisms of void generation and growth in the CWR process for various alloys [9]. Wang et al. established a FEM model to predict the microstructure evolution and mean grain size distribution during the CWR process [10]. Pater et al. numerically studied the CWR of ball pins and found it fully justified [11]. Response surface methodology was used by Lee et al. to optimize the CWR process to prevent formation of Mannesmann hole defect [12]. Jia et al. presented the distribution coefficient of area reduction to analyze the necking in twice-stage CWR [13]. Zhou et al. studied the effect of tool parameters on the tool wear [14].

The scope of the published studies has been limited to low strength materials such as lead [3], aluminum [6], brass [6], and carbon steel [1] with least attention to investigating the CWR process for superalloys. In this paper, the effects of

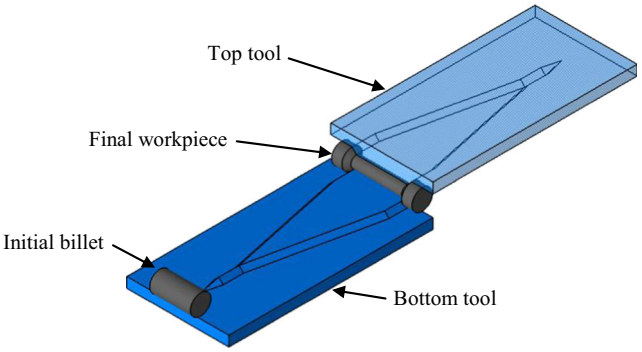

Fig. 1 Diagram of the CWR process

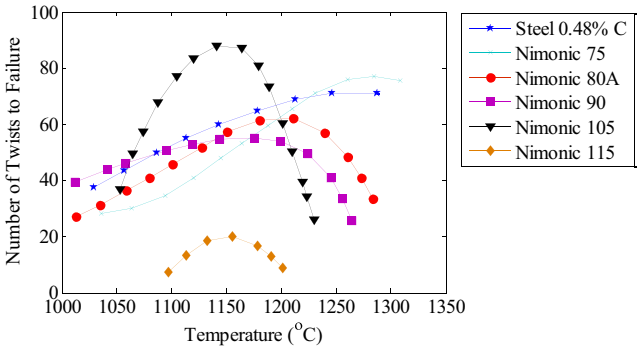

Fig. 3 Hot torsion data for a range of Nimonic® superalloys showing the reduction in ductility [21]

various CWR tool parameters on formability of Nimonic® 80A and Nimonic® 115, two nickel-based superalloys, are presented. First, simulation of CWR process by using finite element method (FEM) is performed. Then, experiments are developed to verify applicability of FEM for this task. The results show that FEM is capable for predicting the necking and slipping of the workpiece. The normalized Cockcroft-Latham model is implemented in FEM to predict the occurrence of internal bursts.

2 CWR process and principles

The CWR tool, as shown in Fig. 1, consists of two wedge shape segments with relative translational or rotational movement toward each other. During the initial stage of CWR process, the tool penetrates into the material to the desired depth and forms a wedge-shaped groove on its circumference. Then the tool spreads the groove to the required width, and finally the desired shape forms. This sequence takes place by four zone of the CWR tool. At the first zone (Fig. 2), knifing zone, a V-shaped groove is formed into the circumference of the workpiece. The desired height reduction is achieved in this zone. Then in the guiding zone, the groove extends to the whole perimeter. In the stretching zone, without change in the height reduction, the width of the groove increases to the desired width. Because some irregularities may form in the workpiece, in the sizing zone, the dimensional tolerance and surface quality of the workpiece are tuned.

There are three common failure modes in CWR process: (1) slipping, (2) necking, and (3) central cavities [15–17]. When the total provocative rotational moment applied to the workpiece is lower than the total preventive rotational moment, the workpiece will slip instead of rotation. If the axial tension stress in the workpiece exceeds the yield strength of the material, necking will occur. The central cavities are one of the most frequent defects limiting CWR process [16]. Central cavity formation in CWR process can be attributed to several possible causes such as (1) large tensile stress in the central portion of the workpiece, (2) excessive shear stresses induced by the first zone of the forming dies, and (3) low cycle fatigue that develops during the rolling process [7]. Central portion of the workpiece is subjected to compression and tension in the directions perpendicular and parallel to the tool surface, respectively. After rotating by 90°, the portions being compressed are subject to tension and vice versa. Such cyclic compression and tension cause fatigue cracks in the material after several rotations of the workpiece [16].

The wedge angle (α) and the stretching angle (β), shown in Fig. 2, are the most important parameters of CWR tool [2]. Improper choosing of α and β in accordance with the relative reduction, $\delta=d_0/d$, results in failing of the workpiece forming (d_0 and d are initial and final diameter, respectively). The wedge angle controls the size of the contact area between the tools and the workpiece in the knifing and stretching zone.

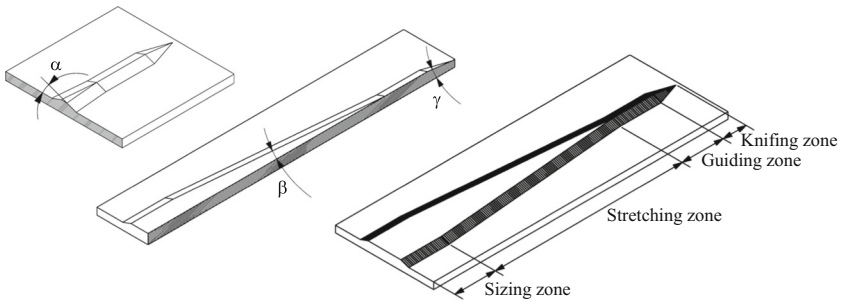

Fig. 2 Geometry of CWR Tool consist of wedge angle (α), stretching angle (β) and ramp angle (γ)

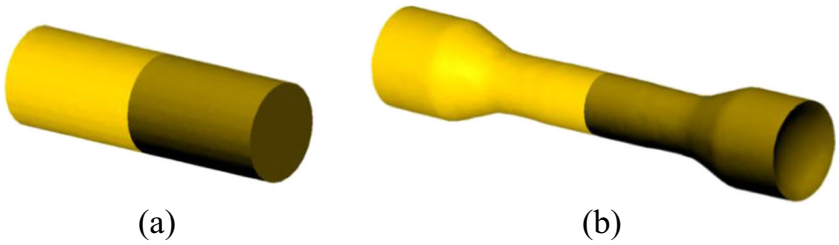

Fig. 4 Due to symmetry, gray portion is omitted from FEM simulations **a** initial billet **b** final part

Smaller wedge angles increase the area contact of the tools and the workpiece and accelerate the formation of internal defects. The large wedge angles increase the probability of necking in the workpiece. Lower values of the stretching angle are associated with a greater length of the tool. For large stretching angles, the billet enlarges rapidly in the axial direction, which accelerates the growth of small internal voids created in the knifing and guiding zones and is considered a potential reason of uncontrolled slip between the rolled workpiece and the tool [7, 8].

To design the CWR tool, Hayama [15] recommended two criteria, namely the wedge angle (α) and stretching angle (β) that should satisfy the conditions described in the formulas (1), (2), and (3):

$$M\beta^{-0.325} \leq 0.15 + 0.0038\alpha \leq 1.93\beta^{-0.725} \quad (1)$$

Where according to the toughness of material, value of M varies between 0.35 and 0.40. The value of M is usually 0.35, but when the material is not tough, it should be larger than 0.35.

Second, the value of reduction in area, R, should be selected in the range of $R_b < R < R_f$, where

$$R_f = 1 - 4\left(2 + \pi\tan\alpha\tan\beta + \sqrt{3\pi/2}cot^{3/2}\alpha\cot^{1/2}\beta/\xi\right)^{-2} \quad (2)$$

and

$$R_b = 1 - (1 + \pi\tan\alpha\tan\beta)^{-2} \quad (3)$$

3 Nickel-base superalloys

Superalloys are a class of materials that retain their properties at highly elevated temperatures. They must have ability to withstand loading at operating temperatures close to their melting point. In addition, resistance to mechanical degradation over long periods is another capability of superalloys. Where resistance to creep along endurance under static loading in high temperature/corrosive conditions is required, the nickel-base superalloys are promising materials. Nimonic® series is a class of nickel-base superalloys, developed in 1940s, for the first generation of gas turbines. However, the application of them is not limited to gas turbines, for example, some metalworking equipments such as forging anvils and extrusion dies are manufactured using Nimonic® series [18, 19].

Nickel-base superalloys have high volume fraction of gamma prime and relatively coarse grain size to improve their creep resistance, so their ductility becomes low. These alloys have relatively narrow hot working temperature range and are sensitive to strain rate and die-chilling effects [20]. Forging nickel-base superalloys needs careful processing to ensure that the workpiece temperature does not exceed low temperature liquation compounds [21]. The results of hot torsion tests to compare the ductility of Nimonic® superalloys are presented in Fig. 3. Figure 3 clearly shows that Nimonic® 115, which has high temperature capability, also exhibit low hot ductility. As seen in Fig. 3, at temperatures above 1,150 °C, the ductility of Nimonic® 115 drops.

Table 1 Parameters used in the simulations

Parameter	Value	Parameter	Value
Wedge angle (α)	15, 20, 25, 30, 35	Initial workpiece temperature (°C)	1,140
Stretching angle (β)	3, 5, 7, 9	Tool temperature (°C)	250
Ramp angle (γ)	7	Environment temperature (°C)	20
Relative reduction (δ)	1.2, 1.4, 1.6, 1.8	Relative tool velocity (m/s)	1
Friction factor (m)	0.2	Initial billet diameter (mm)	40

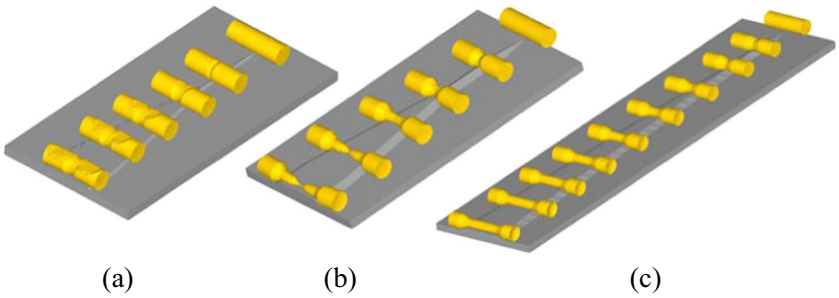

Fig. 5 Steps of workpiece deformation during CWR process, **a** slipping of workpiece between tools, **b** necking of the workpiece, and **c** proper forming of the workpiece

4 FEM simulations

4.1 Outline of the model

A coupled thermal-mechanical finite element method (FEM) model is developed based on viscoplastic model of material using commercially available software [22]. The flow of material in CWR process is complex and cannot be modeled as a 2D model of plane strain or axisymmetric. Given the longitudinal symmetry of the selected geometry and in order to minimize the time required to simulate the process, only one half of the workpiece is modeled (Fig. 4). On the plane of symmetry, the longitudinal displacement of the nodes is constrained. The workpiece is discretized by 20,000 tetrahedral elements. In addition, the tools are considered rigid, and shear model of friction with constant friction factor is used during the process. The heat transfer coefficient between Nimonic® 115, Nimonic® 80A, and die are considered to be 3,000 W/K/m^2. Except the symmetry plane, all of the free surfaces of the workpiece undergo convection heat transfer to ambient under a convection coefficient of 20 W/K/m^2 determined by inverse method. Because of the fast linear motion of the tools, the temperature change of the tools is low and has no considerable effect on the flow of the billet. So, the tool temperature is assumed constant during the simulation.

To investigate the effect of CWR tool parameters leading to successful forming of the workpiece, a series of simulations are performed considering the parameters depicted in Table 1. The workpiece materials are Nimonic® 80A and Nimonic® 115, where all of the tabulated parameters are the same for both materials. The flow behavior of Nimonic® 80A and Nimonic® 115 are extracted from the published literature [23, 24].

According to the process parameters, workpiece necking or slipping may occur. FEM simulation is utilized to predict these instabilities. If the tool parameters are chosen properly, the initial billet without slipping or necking will rotate and form a sound part. Otherwise, the workpiece may neck or slip. In Fig. 5, gradual forming of the workpiece, necking, and slipping are illustrated.

Since superalloys have relatively narrow hot working temperature range, it is required to assess the temperature changes during the CWR process. In Fig. 6, the distribution of the temperature at the end of guiding zone for various δ and α= 20° for Nimonic® 115 is shown. Increasing δ is corresponding to more deformation and growth of temperature rise.

4.2 Predicting of central bursts occurrence

In metal forming practices, the main issue is predicting the location of fracture initiation and the level of deformation at which cracking can occur. Because of different tool and workpiece geometries and diversity in the method of applying force, each metal forming practice may have a different stress state. Since stress in the material considerably determines evolution of ductile damage within the deforming workpiece,

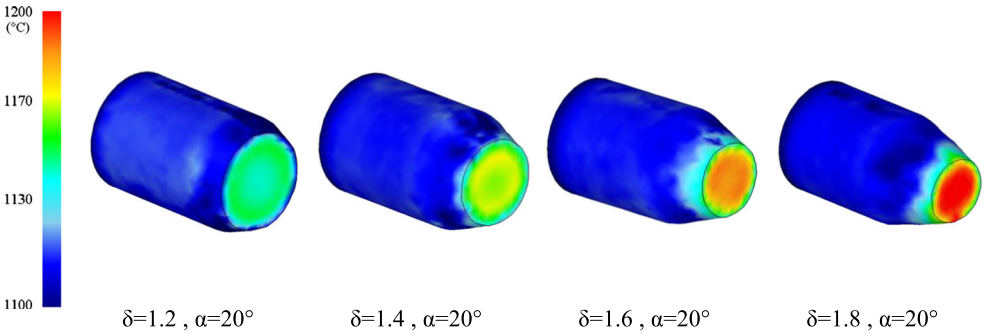

Fig. 6 Distribution of temperature at the end of the guiding zone for various combination of relative reduction (δ) and α=20° for Nimonic® 115

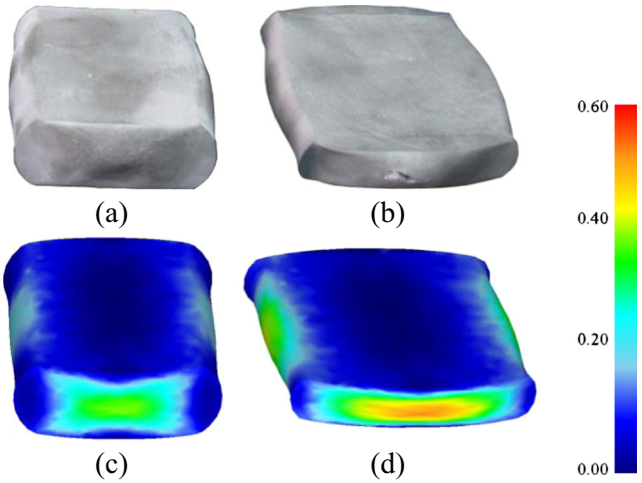

Fig. 7 Side-pressed sample to different height **a** height reduction from 50 to 20 mm, **b** fracture of the sample at height reduction from 50 mm to 9 mm, and **c, d** damage distribution in the sample

in order to predict the probability of void initiation, several damage models are developed [25–28]. Cockcroft-Latham model is a damage model that in addition to cold bulk metal forming [29, 30] and sheet metal forming [31, 32], has been implemented in hot metal forming to predict the failure occurrence [30, 33, 34]. Normalized Cockcroft-Latham damage is based on the tensile strain energy per unit of volume and can be expressed as [28],

$$\int_0^{\bar{\varepsilon}_f} \frac{\sigma^*}{\bar{\sigma}} d\bar{\varepsilon} = C_1 \tag{4}$$

where $\bar{\varepsilon}_f$ is the fracture strain, $\bar{\sigma}$ is the equivalent stress, σ^* is the highest tensile stress, $\bar{\varepsilon}$ is the equivalent strain and C_1 is the normalized critical damage value. In the present study, the normalized Cockcroft-Latham critical damage value of Nimonic® 115 is determined by performing a series of side-pressing tests supplementing the FEM simulations. In these tests, billets having diameter of 50 mm and length of 65 mm are side-pressed to different heights at temperature of 1,140 °C. At the height that fracture appeared, the normalized critical damage was determined by corresponding FEM simulation. According to the performed tests, the normalized critical damage value of Nimonic® 115 is equal to 0.6. In Fig. 7, side-pressed samples at two height reductions and corresponding FEM distribution of normalized C-L damage are shown.

In this paper, the normalized Cockcroft-Latham damage model is implemented to simulate the process leading to the central burst defects. The study of the damage value at the various combinations of the tool parameter shows that for some combinations, before entering the workpiece to the stretching zone, the damage parameter reaches the normalized critical damage and results in the central bursts. Distribution of damage value for various relative height reduction (δ) and α= 20° for Nimonic® 115 at the end of the guiding zone is shown in Fig. 8.

5 Experimental works

A series of experiments are performed to investigate the CWR process for superalloys Nimonic® 80A and 115. The experimental parameters are the same as those tabulated in Table 1; however, further explanations are brought here for sake of clarity. In these experiments, billets with chemical composition shown in Table 2 are used with initial microstructure of the materials in Fig. 9.

The apparatus that is used in this study is an industrial machine that has the capacity of 2,000 and 120 kN in radial and tangential directions, respectively. Speed of the tool slides during the rolling is variable with maximum 500 mm/s. The workpieces are preheated in an electrical furnace to temperature of 1,140 °C and are maintained for 15 min to find a uniform temperature. In addition to wedge serrations, two side serrations are inserted in the beginning of the knifing zone to prevent the initial slip between the workpiece and the tool as shown in Fig. 10. To reduce the heat loss of the workpieces,

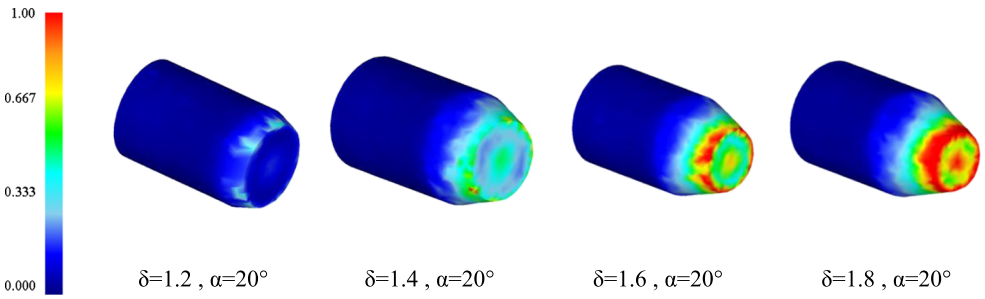

Fig. 8 Distribution of normalized Cockcroft-Latham damage at the end of the guiding zone for various δ value and α=20° for Nimonic® 115

Table 2 Chemical composition of materials used in the experiments

Nimonic® 80A	Cr	Ti	Al	Fe	Co	Mn	Si	Ni	
	20.0	2.5	1.5	1.0	1.0	0.5	0.5	Base	
Nimonic® 115	Cr	Co	Ti	Al	Fe	Mo	C	Si	Ni
	15.0	14.2	4.2	4.7	0.3	4.1	0.18	0.2	Base

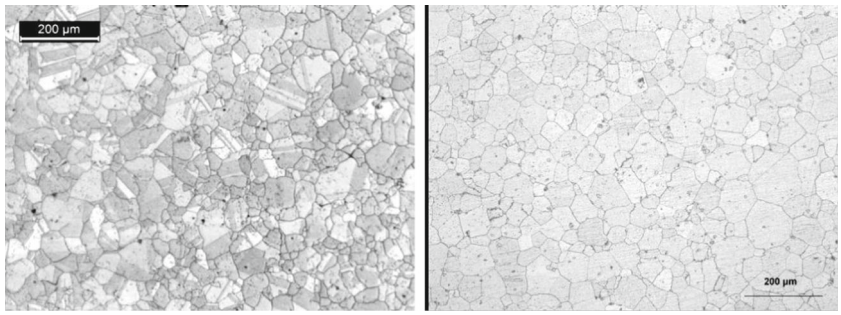

(a) (b)

Fig. 9 Microstructure of initial billet (×100): **a** Nimonic® 80A and **b** Nimonic® 115

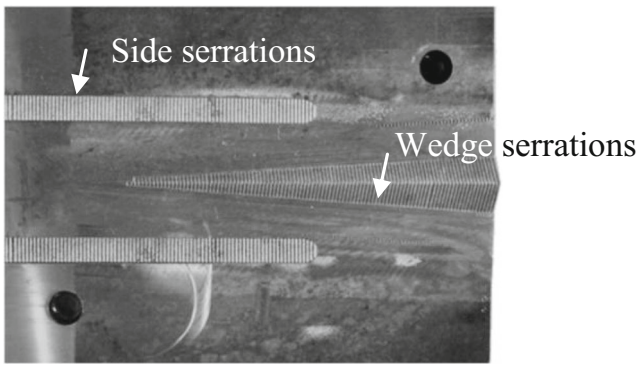

Fig. 10 Knifing zone of the tool including wedge and side serrations

Deltaglaze, a lubricant that acts as a heat transfer barrier is applied to the surface of the workpiece. The tools are heated to 250 °C and the relative speed of the tool slides is set to 1 m/s.

Experimental result with parameters δ=1.6, α=15°, and temperature=1,140 °C for Nimonic® 115 (Fig. 11b) reveals that in the middle of the guiding zone, the workpiece internally bursts. It can be said that due to limited rotation of the workpiece, low cycle fatigue does not occur and internal burst is the result of tensional stresses. Related normalized Cockcroft-Latham damage distribution is depicted in Fig. 11a. The corresponding normalized damage value in the FEM simulation at the middle of the guiding zone is 0.58 and is approximately equal to the normalized critical damage value that was determined by side-pressing tests. This result is in good agreement with the predicted central burst by FEM simulation, so regardless of the β value, for δ=1.6 and α=15°, central burst may occur. In Figs. 12 and 13, the results of experiments with tool parameters of δ=1.8, α=30°, and β=7° and δ=1.6, α=30°, and β=5° for Nimonic® 115 are shown, respectively. In these cases, the FEM simulation precisely predicts the occurrence of workpiece necking.

Experimental results on the Nimonic® 80A shows that in some situations not meeting Hayama's criteria, this material forms properly. Two combinations of tool parameters, not recommended by Hayama but results in sound workpiece is δ=1.8, α=15°, β=5° and δ=1.6, α=15°, β=3°. The corresponding workpieces are illustrated in Figs. 14 and 15.

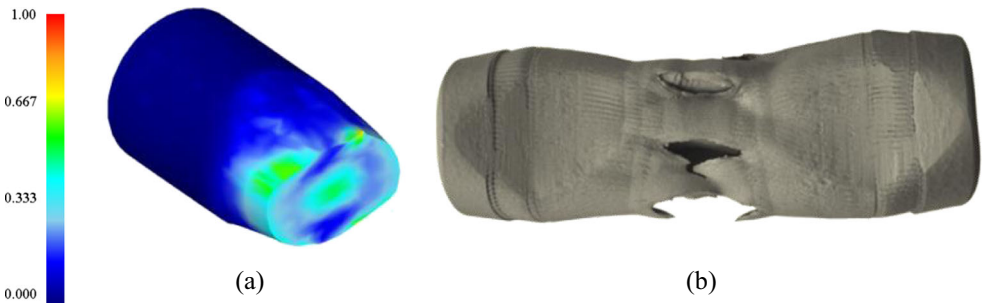

(a) (b)

Fig. 11 **a** distribution of the normalized C-L damage in cross wedge rolled workpiece of Nimonic® 115 with δ=1.6, α=15°, and temperature=1,140 °C at the middle of guiding zone, **b** corresponding experiment

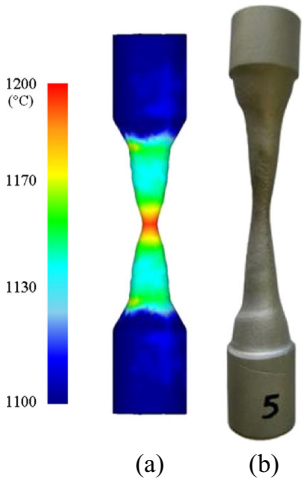

Fig. 12 Necked C.W. Rolled workpiece, material: Nimonic® 115, δ=1.8, α=35°, β=5°, and initial temperature=1,140 °C **a** distribution of temperature in FEM simulation, **b** experiment

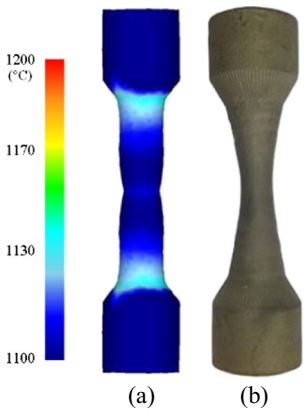

Fig. 13 Necked C.W. Rolled workpiece, material: Nimonic® 115, δ=1.6, α=30°, β=5°, and initial temperature=1,140 °C **a** distribution of temperature in FEM simulation, **b** experiment

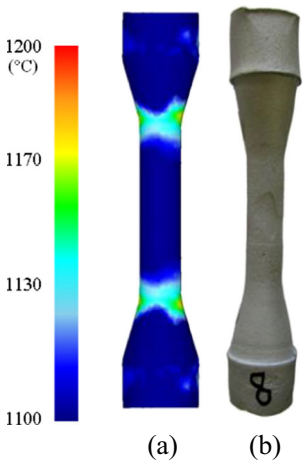

Fig. 14 Sound C.W. Rolled workpiece, material: Nimonic® 80A, δ=1.8, α=15°, β=5°, and initial temperature=1,140 °C **a** distribution of temperature in FEM simulation, **b** experiment

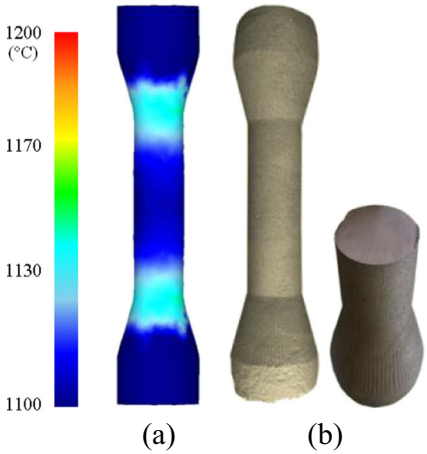

Fig. 15 Sound cross wedge rolled workpiece of Nimonic® 80A, δ=1.6, α=15°, β=3°, and initial temperature=1,140 °C **a** distribution of temperature in FEM simulation, **b** experiment

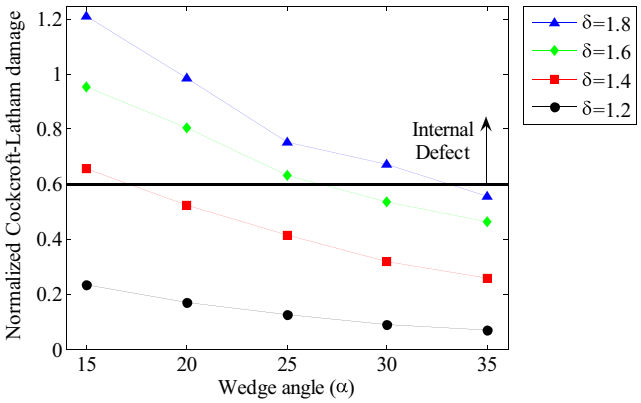

Fig. 16 Interaction plot of effect of α and δ on damage parameter at the end of the guiding zone for Nimonic® 115

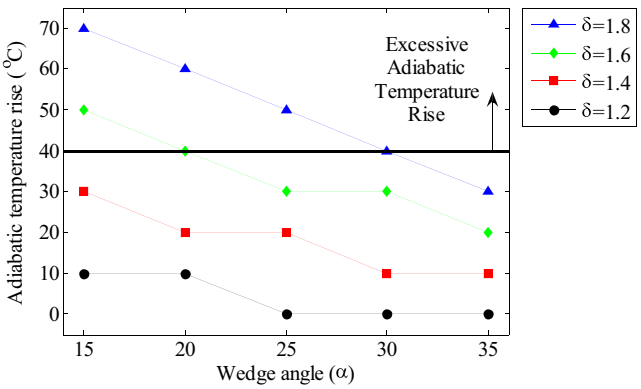

Fig. 17 Interaction plot of effect of α and δ on the adiabatic temperature rise for Nimonic® 115

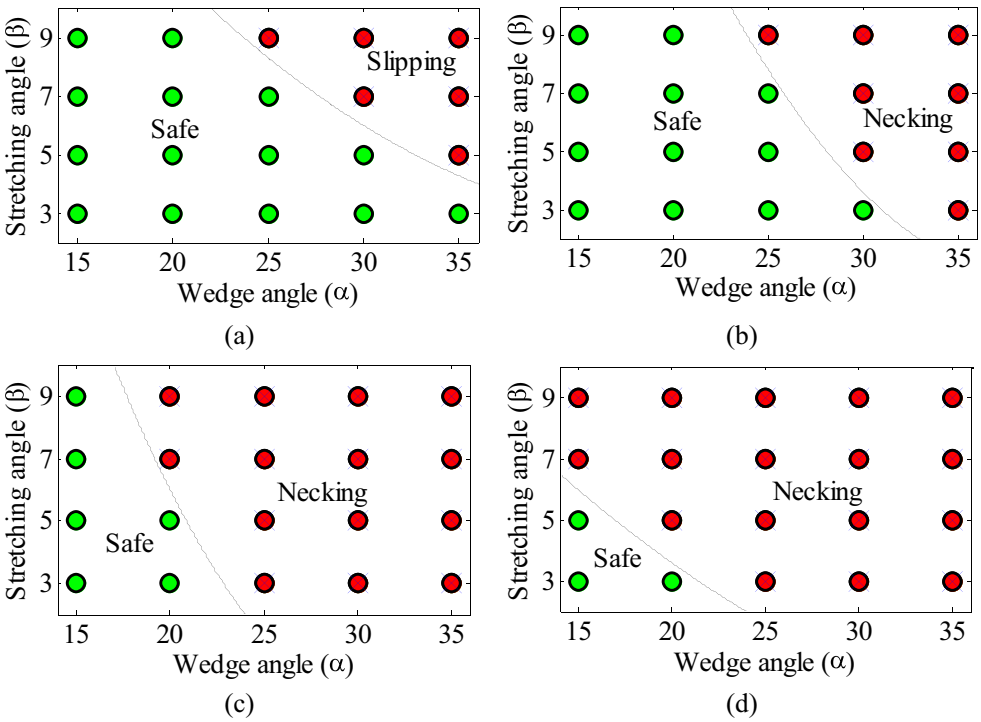

Fig. 18 Summary of tool parameter results for Nimonic® 80A, **a** δ=1.2, **b** δ=1.4, **c** δ=1.6, and **d** δ=1.8

6 Results and discussion

A set of simulations according to Table 1 are performed and formability of Nimonic® 80A and Nimonic® 115 by CWR process is investigated. As shown in Fig. 11, for Nimonic® 115, the workpiece may internally burst before entering the stretching zone. Therefore, regardless of β value, internal burst may form in the workpiece. In Fig. 16, interaction plot of the effect of α and δ on the damage parameter, at the end of guiding zone is illustrated. According to Fig. 16, by decreasing the δ and increasing α value, the damage value decreases and probability of internal bursts declines. As shown in Fig. 16, for some combinations of α and δ, regardless of the β value, the damage value is more than the critical damage and may result in central bursts.

As described, adiabatic temperature rise is another limiting criterion in forming superalloys. Nimonic® 115 has a narrow window of ductility and adiabatic heating of the workpiece during the forming process may result in melting of low temperature liquation compounds. Temperature rise or drop during the forming process has a significant effect on the resultant workpiece. In Fig. 6, the distribution of the temperature at the end of guiding zone for various δ and α=20° is shown. The results show that with increase in relative reduction (δ) and decrease of wedge angle (α), adiabatic temperature rise increases. In addition, results show that because of gradual forming in the stretching zone, maximum temperature rise occurs before stretching zone. So interaction plot of the effect of δ and α on adiabatic temperature rise at the end of the guiding zone is presented in Fig. 17. Increasing δ and decrease in α, augments the adiabatic temperature rise. As shown in Fig. 17, some combinations of δ and α result in the process temperature exceeding workability window of Nimonic® 115.

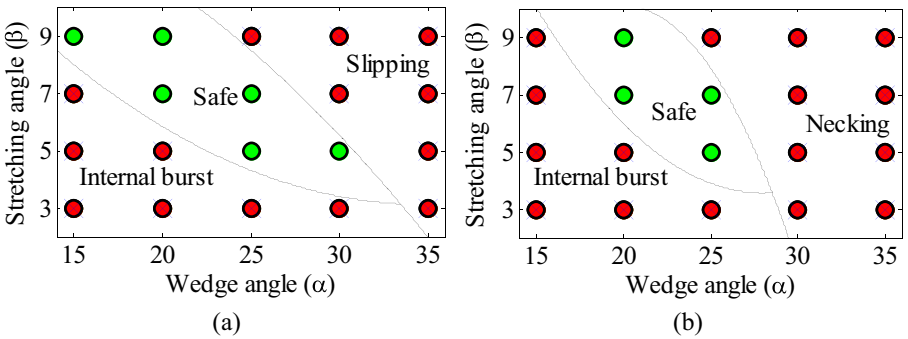

Fig. 19 Summary of tool parameter results for Nimonic® 115, **a** δ=1.2, and **b** δ=1.4

The summary of simulations results with the parameters given in Table 1, for Nimonic® 80A and Nimonic® 115 are presented in Figs. 18 and 19, respectively. Decrease in δ and increase of α result in reduction of the contact area between the tool and the workpiece. For both superalloys, δ=1.2 and larger wedge angles lead to slipping of the workpiece. Decreasing of α and β may prevent slipping, but by decreasing α for Nimonic® 115, damage value increases and may result in internal burst. Experimental results show that Nimonic® 80A is resistant to forming internal burst even in severe cases such as Fig. 14.

With increasing δ, tool parameter combinations that lead to necking spread out. Figure 18 shows that for Nimonic® 80A and δ=1.8, only limited cases produce sound part. For Nimonic® 115, because of internal defect formation, suitable tool parameters are very limited. Decreasing α and β rises probability of internal burst occurrence. For Nimonic® 115, all tool parameter combinations of δ=1.6 or 1.8 fail to form a sound part.

7 Summary and conclusion

This article discussed a study on the effect of CWR tool parameters on formability of Nimonic® 80A and Nimonic® 115 superalloys. Normalized Cockcroft-Latham model is implemented through FEM to predict the probability of occurrence of internal bursts. The FEM is capable to predict the effects of slipping and necking of the workpiece. Experimental results producing burst and necking phenomena validated the numerical results. Summary of the conclusions are the following:

- For material Nimonic® 115, for some combinations of relative reduction (δ) and wedge angle (α) regardless of stretching angle (β), the central burst causes failure in forming of the workpiece.
- Because Nimonic® 115 has a limited ductility, the combinations of tool parameters that lead to sound part for Nimonic® 115 is very limited compared with Nimonic® 80A.
- For Nimonic® 115, relative reduction of δ=1.6 or more results in filature of sound part forming.
- For tool parameter of low α and low β, Nimonic® 80A is resistant to formation of internal bursts.

The results contribute to better understanding of Ni-base superalloys in CWR process and can lead to manufacturing hot parts of gas turbines with a low-cost and high-productivity process.

References

1. Pater Z (2000) Theoretical and experimental analysis of cross wedge rolling process. Int J Mach Tool Manuf 40(1):49–63
2. Dong Y, Lovell M, Tagavi K (1998) Analysis of interfacial slip in cross-wedge rolling: an experimentally verified finite-element model. J Mater Process Technol 80–81:273–281
3. Pater Z (1997) Theoretical method for estimation of mean pressure on contact area between rolling tools and workpiece in cross wedge rolling processes. Int J Mech Sci 39(2):233–243
4. Lovell MR (2001) Evaluation of critical interfacial friction in cross wedge rolling. J Tribol-Trans ASME 123(2):424–429
5. Pater Z (1999) Numerical simulation of the cross wedge rolling process including upsetting. J Mater Process Technol 92:468–473
6. Deng Z, Lovell MR, Tagavi KA (2001) Influence of material properties and forming velocity on the interfacial slip characteristics of cross wedge rolling. J Manuf Sci Eng 123(4):647–653
7. Li Q, Lovell MR, Slaughter W, Tagavi K (2002) Investigation of the morphology of internal defects in cross wedge rolling. J Mater Process Technol 125–126:248–257
8. Pater Z (2003) Tools optimisation in cross wedge rolling. J Mater Process Technol 139(1):153–159
9. Li Q, Lovell MR (2004) The establishment of a failure criterion in cross wedge rolling. Int J Adv Manuf Technol 24(3–4):180–189
10. Wang M, Li X, Du F, Zheng Y (2004) Hot deformation of austenite and prediction of microstructure evolution of cross-wedge rolling. Mater Sci Eng A-Struct Mater 379(1):133–140
11. Pater Z, Bartnicki J, Samolyk G (2005) Numerical modelling of cross-wedge rolling process of ball pin. J Mater Process Technol 164:1235–1240
12. Lee HW, Lee GA, Yoon DJ, Choi S, Na KH, Hwang MY (2008) Optimization of design parameters using a response surface method in a cold cross-wedge rolling. J Mater Process Technol 201(1):112–117
13. Jia Z, Zhou J, Ji J, Lei Z, Xiang D, Sun X (2013) Influence analysis of area reduction for necking in twice-stage cross wedge rolling. Int J Adv Manuf Technol 66(9–12):1407–1413
14. Zhou J, Xiao C, Yu Y, Jia Z (2013) Influence of tool parameters on tool wear in two-roll cross-wedge rolling. Int J Adv Manuf Technol 65(5–8):745–753
15. Hayama M (1979) Optimum working conditions in the cross rolling of stepped shaft. J Mech Work Technol 3(1):31–46
16. Pater Z, Weroński W, Kazanecki J, Gontarz A (1999) Study of the process stability of cross wedge rolling. J Mater Process Technol 92–93:458–462
17. Dong Y, Tagavi KA, Lovell MR (2000) Analysis of interfacial slip in cross-wedge rolling: a numerical and phenomenological investigation. J Mater Process Technol 97(1):44–53
18. Reed RC (2006) The superalloys fundamentals and applications. Cambridge University Press
19. Betteridge W, Heslop J (1974) The Nimonic alloys and other nickel-base high-temperature alloys. Edward Arnold Press
20. Wright DC, Smith DJ (1986) Forging of blades for gas turbines. J Mater Sci Technol 2(7):742–747
21. Brooks JW (2000) Forging of superalloys. J Mater Des 21(4):297–303
22. DEFORM-3D User's Manual (2009) Scientific Forming Technologies Corporation
23. Shahriari D, Sadeghi MH, Akbarzadeh A, Cheraghzadeh M (2009) The influence of heat treatment and hot deformation conditions on γ′ precipitate dissolution of Nimonic 115 superalloy. Int J Adv Manuf Technol 45(9–10):841–850

24. Jeong HS, Cho JR, Park HC (2005) Microstructure prediction of Nimonic 80A for large exhaust valve during hot closed die forging. J Mater Process Technol 162:504–511
25. Freudenthal AM (1950) The inelastic behavior of solids. Wiley
26. Oyane M (1972) Criteria of ductile fracture strain. Bull JSME 15(90): 1507–1513
27. Rice JR, Tracey DM (1969) On the ductile enlargement of voids in triaxial stress fields. J Mech Phys Solids 17(3):201–217
28. Cockcroft MG, Latham DJ (1968) Ductility and the workability of metals. J Inst Met 96(1):33–39
29. Landre J, Pertence A, Cetlin PR, Rodrigues JMC, Martins PAF (2003) On the utilisation of ductile fracture criteria in cold forging. Finite Elem Anal Des 39(3):175–186
30. Quan GZ, Wang FB, Liu YY, Shi Y, Zhou J (2013) Evaluation of varying ductile fracture criterion for 7075 aluminum alloy. T Nonferrous Metal Soc 23(3):749–755
31. Takuda H, Mori K, Hatta N (1999) The application of some criteria for ductile fracture to the prediction of the forming limit of sheet metals. J Mater Process Technol 95(1):116–121
32. Ozturk F, Lee D (2004) Analysis of forming limits using ductile fracture criteria. J Mater Process Technol 147(3):397–404
33. Nicolaou PD, Semiatin SL (2005) An analysis of cavity growth during open-die hot forging of Ti-6Al-4 V. Metall Mater Trans A 36(6):1567–1574
34. Kukuryk M (2012) Analysis of deformation and damage evolution in hot elongation forging. Arch Metall Mater 55(2):417–424